Electrochemical Hydrogen Charging of Duplex Stainless Steel

L. Claeys,[‡,*] T. Depover,[*] I. De Graeve,[**] and K. Verbeken[*]

[‡]Corresponding author. E-mail: Lisa.Claeys@UGent.be.

[*]Ghent University, Department of Materials, Textiles and Chemical Engineering, Tech Lane Ghent Science Park–Campus A, Technologiepark 46, 9052 Zwijnaarde, Belgium.

[**]Vrije Universiteit Brussel, Department of Materials and Chemistry, Pleinlaan 2, 1050 Brussels, Belgium.

Article Citation:

ABSTRACT

This study evaluates the electrochemical hydrogen charging behavior and interaction between hydrogen and the microstructure of a duplex stainless steel. A saturation level of approximately 650 wppm is reached after 10 d of charging. The data are compared with a model resulting in a diffusion coefficient of 2.1×10^{-14} m²/s. A two-step increase of the concentration is observed and ascribed to saturation of ferrite followed by charging of austenite grains. Microstructural changes are observed during charging, i.e., formation and interaction of dislocations, as a result of the high residual stresses inherent to the production process of duplex stainless steels.

KEY WORDS: diffusion, duplex stainless steels, hydrogen absorption, plastic deformation

INTRODUCTION

Duplex stainless steels (DSS) are characterized by a two-phase microstructure of austenite (γ) with a face-centered cubic (FCC) crystal structure and ferrite (α) with a body-centered cubic (BCC) crystal structure, ideally in equal fractions. Consequently, the properties of DSS are a mixture of the properties of ferrite and austenite. They are typically stronger and more stress corrosion cracking resistant than austenitic steels and tougher than ferritic steels. The use of DSS has largely increased during the last decade due to their good mechanical properties with main applications in oil and gas, paper, and the chemical industry.[1] However, these duplex stainless steels suffer in specific combinations of hydrogen, chemical composition, and mechanical stress from hydrogen embrittlement (HE), i.e., a deterioration of the metal's mechanical properties caused by the presence of hydrogen inside the microstructure.[2] Galvanic coupling with low carbon steel and cathodic corrosion protection are some examples that might cause DSS to suffer from HE. In both situations, the DSS will act as cathode leading to a hydrogen evolution and subsequent absorption into the steel microstructure.[3]

The two-phase austenite/ferrite microstructure of DSS complicates the study or prediction of the HE susceptibility due to the large discrepancies between both phases in terms of their interaction with hydrogen. Austenite is characterized by a high hydrogen solubility together with a low hydrogen diffusivity, whereas ferrite shows a low hydrogen solubility and a high hydrogen diffusivity.[4] Recently, the HE sensitivity of BCC steel types was already the subject of multiple studies[5-7] and it is generally accepted that diffusible hydrogen is mainly responsible for the obtained degree of HE.[8] Apart from the amount of diffusible hydrogen, the hydrogen diffusion coefficient also was confirmed to play a determinant role.[9] Consequently, FCC steels were at some point considered insensitive to HE because of their low hydrogen diffusivity.[10] However, a hydrogen-induced ductility loss has already been demonstrated in austenitic steels,[11-12] resulting in an increased interest toward HE research of duplex and austenitic stainless steel types.[13-14]

Multiple studies pointed out that austenitic steels might be subjected to microstructural changes due to hydrogen charging. For instance, Yang and Luo[15] stated that a critical current density exists at which α'-martensite (body-centered tetragonal, BCT) or ε-martensite (hexagonal closed packed, HCP) formation takes place during hydrogen charging and subsequent outgassing of austenitic stainless steel. For every current density above this critical value, martensite formation takes place after a certain charging time. This charging time decreases with increasing current density. The authors assumed that α'-martensite did not form during the charging procedure, but only after a certain outgassing time. However, ε-martensite was observed immediately after charging. Glowacka, et al.,[16] stated that the orientation relationship between austenite and ferrite grains might be important for α'-martensite formation as favorably oriented ferrite grains can serve as nuclei for the transformation of austenite to α'-martensite. Furthermore, Dabah, et al.,[17] demonstrated that hydrogen desorption induced surface tensile stresses provoking the phase transformation γ → ε → α'. Martensitic phases induced by hydrogen charging and desorption were also observed by Glowacka, et al.,[18] and they correlated this transformation with the degradation of a theoretical FCC hydride phase created in austenite, which has an increased cell parameter because of hydrogen presence, or with the hydrogen-induced plastic strain. Apart from martensitic transformations, other microstructural changes were observed as well. Barnoush, et al.,[19] observed slip band formation on the surface of the austenite phase in a super DSS via atomic force microscopy during in situ hydrogen charging. Observations were thus done on the level of individual grains. The phenomenon was explained by the nucleation and migration of dislocations. Luo, et al.,[20] combined electron backscatter diffraction (EBSD) and electron channeling contrast imaging (ECCI) and observed stacking fault formation in the austenite grains and an increase in dislocation density in ferrite after hydrogen charging of a DSS. Finally, Liang, et al.,[21] observed an increase in dislocation density of both austenite and ferrite in a super DSS after hydrogen charging. The dislocation density was determined via time-of-flight (ToF) neutron diffraction which provides information on bulk

properties due to the large penetration depth of the used neutrons. When prestrain was applied to the DSS, the increase of the dislocation density in both ferrite and austenite due to hydrogen was rather limited.

Despite the complicated interaction of hydrogen with the microstructure during the charging procedure, DSS were charged with hydrogen in the past decade in order to evaluate their HE susceptibility. A large variety of environments was used to accomplish this. On the one hand, gaseous hydrogen charging at an elevated temperature is possible. San Marchi, et al.,[22] used, e.g., 138 MPa H_2 gas at 573 K and charged 125 wppm in a 2507 DSS plate after 10 d. El-Yazgi and Hardie[23] used 22 MPa H_2 gas at 623 K for 48 h and charged 20 wppm in a 2205 DSS. On the other hand, electrochemical hydrogen charging with various electrolyte solutions is an option as well. Zakroczymski, et al.,[24] were able to charge 208 wppm in a 2.1 mm diameter UNS S31308 DSS bar using 0.1 M H_2SO_4 with 10 mg/L As_2O_3 as electrolyte and a current density of 20 mA/cm² for 2 weeks. Other electrolytes were also used these the authors, but less hydrogen was charged into the steel for the same charging time. The authors pursued a charging time that was assumed to result in saturation of both the ferrite and austenite phase fraction via diffusivity-based calculations, but they did not confirm saturation experimentally. Dabah, et al.,[17] charged 156 wppm in a 0.6 mm SAF 2507 DSS plate using a 0.25 M H_2SO_4 electrolyte solution with 0.25 g/L $NaAsO_2$ at 50 mA/cm² for 72 h. Shorter charging times were tested as well. The hydrogen content still showed an increasing trend after 72 h of charging meaning that saturation was not yet reached. Luo, et al.,[20] charged a 0.5 mm 2205 DSS plate in 0.5 M H_2SO_4 with 0.25 g/L As_2O_3 at 1.5 mA/cm². The hydrogen evolution at a constant temperature of 50°C amounted to 8.5 wppm after 2 d of charging. Griffiths and Turnbull[25] stated that hydrogen contents between 100 wppm and 250 wppm were needed in a 22% Cr duplex stainless steel to cause environment-assisted cracking after charging at 80°C in an acid brine environment.

A wide variety of hydrogen levels can be found in literature for hydrogen-charged DSS depending, among other things, on charging time, sample size, environment type, current density, and the hydrogen detection method. Saturation was never confirmed by means of experiments at different charging times. Moreover, in many studies, saturation, despite being very relevant, was no necessity to draw conclusions on the influence of hydrogen on various properties. The aim of the present work is therefore to construct a complete saturation curve for electrochemical hydrogen charging of UNS S32205 DSS and combine this with a study of the microstructural changes taking place due to the interaction of hydrogen with the microstructure upon electrochemical charging.

EXPERIMENTAL PROCEDURE

Material Characterization

The used material was an UNS S32205 duplex stainless steel. The as-received plate had a thickness of 4 mm and underwent a 60% thickness reduction by cold rolling. The cold rolled steel was annealed at 1,100°C for 1 h to erase the microstructural effects of cold rolling. The composition of the industrial UNS S32205 duplex stainless steel is given in Table 1.

TABLE 1. Chemical Composition of UNS S32205

Wt%	C	Cr	Ni	Mo	Mn	Other
UNS S32205	0.013	22.45	5.31	2.63	1.81	Cu 0.24, P 0.02, S 0.0005 Si 0.38

Microstructural characterization was performed with optical microscopy and scanning electron microscopy (SEM). The used optical microscope was a Keyence VHX-S90BE. The VHX software (VHX-2000E) of the optical microscope was used to determine phase fractions based on the difference in brightness. A FEI Quanta 450 SEM with field emission gun (FEG) was used with an accelerating voltage of 20 kV and a spot size of 5 nm. Standard metallographic sample preparation was performed including grinding and polishing. Chemical etching was performed for visualization of the microstructure (Carpenters' etchant, i.e., 8.5 g $FeCl_3$, 2.4 g $CuCl_2$, 122 mL HCl, 6 mL HNO_3, and 122 mL ethanol). Additionally, EBSD was used to study the different phases present in the steel before and after hydrogen charging. OP-U (colloidal silica, 0.04 µm) was used as a final step instead of chemical etching to create flat surfaces as required for EBSD.[26] EBSD measurements were performed on the mentioned SEM using a tilt angle of 70° and a step size ranging from 0.05 µm to 0.10 µm on a hexagonal grid. TSL-OIM Data analysis V7.3 software was used for post processing and analysis of the crystallographic orientation data. Inverse pole figure (IPF) maps and phase maps were created. High-angle grain boundaries (greater than 15°) were indicated by black lines while low-angle grain boundaries (5° < θ < 15°) were indicated by white lines.

Hydrogen Characterization

Electrochemical hydrogen charging was performed at a constant current density of 0.8 mA/cm² in an 0.5 M H_2SO_4 electrolyte solution containing 1 g/L thiourea, which was added as a poison to reduce the recombination of adsorbed hydrogen atoms into H_2. The DSS sample acted as the cathode while platinum foils, present at both sides of the sample, were used as anode. These conditions were already used in hydrogen research on BCC steels in the research group before.[6] Prior to hydrogen charging, the thickness of the material was reduced by grinding in order to be able to saturate the steel. Moreover, grinding minimized the surface oxide layer. Metal oxides, including those of steel, are stated to have an inhibiting effect on hydrogen absorption reducing the hydrogen permeability with at least one order of magnitude.[8] The final steel plate thickness after grinding was 0.3 mm with an accuracy of ± 10 µm. The other dimensions were 8 mm × 6 mm. Hydrogen was introduced perpendicular to the elongated grain structure.

The total hydrogen content charged into the DSS plate was determined after different applied charging times. This was accomplished by melting small rectangles (6 mm × 8 mm) at 1,550°C in a Galileo G8 set-up operated with an impulse furnace for heating and a thermal conductivity detector (TCD) for hydrogen detection. At least three tests were performed for every applied charging time to obtain confirmation of the obtained research.

RESULTS

An optical microscopy image of the initial microstructure is shown in Figure 1(a). The two phases are clearly distinguishable, i.e., the lighter parts are austenite grains and the darker fraction is the ferrite phase. The overall structure is elongated in the rolling direction which is typical for duplex stainless steels.[1] The ferrite phase fraction forms a continuous network through the thickness of the material and the austenite grains form islands in the ferrite matrix. The phase balance was determined with the VHX software based on the difference in brightness on various optical images. This resulted on average in an austenite fraction of 50.0 % ± 1.5 %. An SEM image of the initial microstructure is shown in Figure 1(b). Figures 2(a) and (b) show the ND IPF map and the phase map of the EBSD measurement performed on the zone in Figure 1(b), respectively. From various EBSD measurements, it was concluded that the structure contained ferrite bands of approximately 8 μm in thickness and austenite bands of approximately 5 μm in thickness measured parallel to the normal direction.
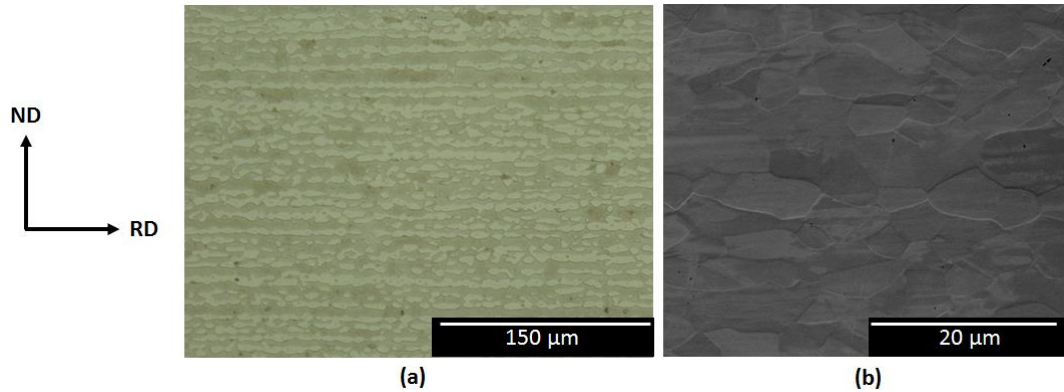

FIGURE 1. Optical and SEM image showing the initial microstructure of UNS S32205 duplex stainless steel.
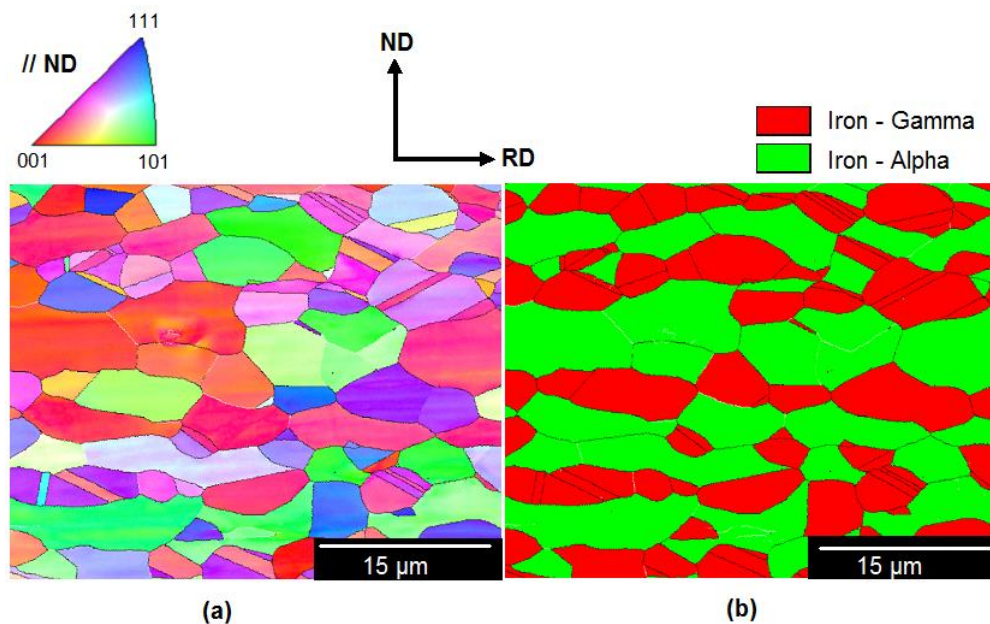

FIGURE 2. Initial microstructure of UNS S32205 DSS: (a) ND IPF map, and (b) Phase map.

The evolution of the total hydrogen content as a function of hydrogen charging time is presented in Figure 3. Hydrogen charging was performed until a saturation level was reached. The increase in hydrogen content was not continuous but showed a change of slope after approximately five days of charging, i.e., a two-step increase of the hydrogen concentration was observed.

A theoretical saturation curve was constructed by solving Fick's second law (1) for one-dimensional diffusion:[27]

$$\frac{\partial C}{\partial t} = D \frac{\partial^2 C}{\partial x^2} \quad (1)$$

where $C(x,t)$ is the hydrogen concentration, x [m] the position, t [s] the time for diffusion, and D [m²/s] the hydrogen diffusion coefficient. Appropriate boundary conditions were chosen by assuming a sheet of thickness 2l with a symmetric concentration profile (2) and by maintaining both surfaces of the sheet at a constant concentration C_0 during the hydrogen charging procedure (3). The latter assumes that the potential remained constant during charging which was also observed during the course of the experiment:

$$\frac{\partial C}{\partial x} = 0, \ x = 0, \ t \geq 0 \ (2)$$

$$C = C_0, \ x = l, \ t \geq 0 \ (3)$$

Solving the one-dimensional diffusion equation with these boundary conditions resulted in a time-dependent expression for the hydrogen concentration profile through the thickness of the material (4):[27]

$$\frac{C}{C_0} = 1 - \frac{4}{\pi}\sum_{n=0}^{\infty}\frac{(-1)^n}{2n+1}\cdot\exp\left(-\frac{(2n+1)^2\cdot\pi^2\cdot D\cdot t}{4l^2}\right)\cdot\cos\left(\frac{(2n+1)\cdot\pi\cdot x}{2l}\right) \quad (4)$$

The total hydrogen concentration as a function of charging time was subsequently calculated by integrating the concentration profile over the given sample thickness and dividing it by the maximal integral 2l. The final equation is given in Eq. (5) where the value of C_0 is replaced by C_{HS}, i.e., the hydrogen saturation level, as this is the maximum concentration that can be reached in the steel:

$$C_H(t) = C_{HS}\cdot(1 - \frac{4}{\pi^2}\sum_{n=0}^{\infty}\frac{(-1)^n}{(2n+1)^2}\cdot\exp(-\frac{(2n+1)^2\pi^2 Dt}{4l^2})\cdot\left(\sin\left(\frac{(2n+1)\pi}{2}\right) - \sin\left(-\frac{(2n+1)\pi}{2}\right)\right) \quad (5)$$

The experimental data were used to fit the two unknown parameters in this equation, i.e., the saturation level C_{HS} and the diffusion coefficient D only considering the first steadily increasing points and the final points when saturation was almost reached. Using all of the experimental data points resulted in a physically impossible fit. The best fit was obtained with a diffusion coefficient of 2.1×10^{-14} m²/s and a saturation level of 650 wppm. These values will be discussed in detail in the next section. The modeled saturation curve is compared to the experimental data in Figure 4.
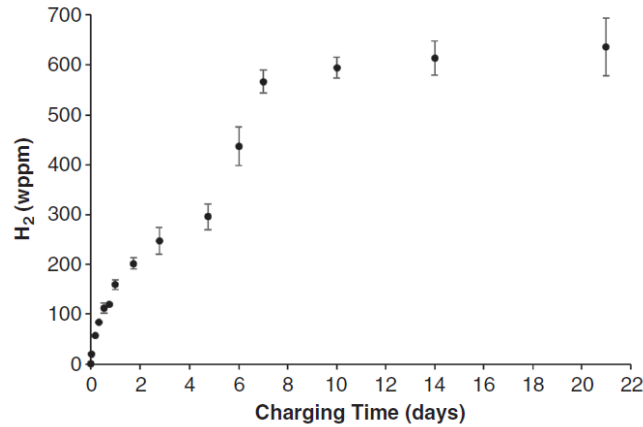

FIGURE 3. Total hydrogen concentration as a function of charging time for UNS 32205 DSS with a thickness of 0.3 mm.
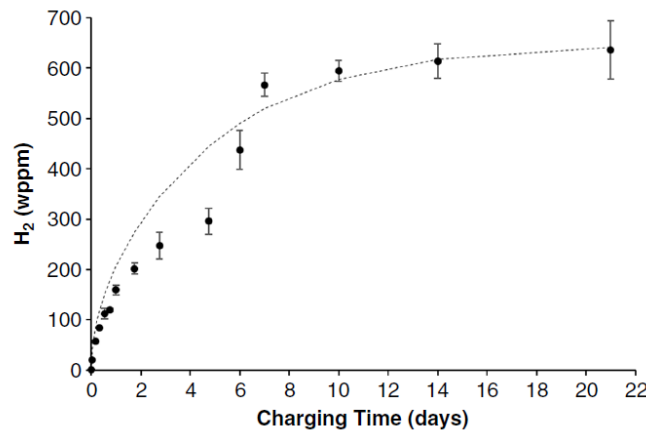

FIGURE 4. Theoretical hydrogen saturation curve (dashed line) based on Fick's second law fitted to experimental data for DSS with a thickness of 0.3 mm.

An in-depth investigation was performed on the hydrogen/material interaction during charging as many authors observed microstructural changes due to the presence of hydrogen.[15,18-20] The microstructural changes as a consequence of hydrogen charging were evaluated for different charging times in our work. After 18 h of hydrogen charging, i.e., in the first increasing part of the curve, a clear surface relief in the austenite phase was observed, as shown in Figure 5, whereas no noticeable changes were seen in the ferrite phase. The microstructural evolution after 1 week of hydrogen charging was evaluated as well, i.e., when the steel is almost saturated with hydrogen. Similar to the results after 18 h of hydrogen charging, a surface relief was observed for the austenite phase. EBSD was used to study the possible presence of both hydrogen-induced α'-martensite and hydrogen-induced ε-martensite. Three different phases were considered as possible in the EBSD software, i.e., γ-iron, α-iron, and ε- martensite. As α'-martensite is very similar to α-iron, this phase could not be loaded separately. In order to obtain high-quality EBSD results, the surface was slightly re-polished after charging, which removed the surface relief. An ND IPF map and phase map of both the surface and cross section of the charged specimen were made, as shown in Figures 6 and 7, respectively. No indications of martensite phases were observed inside γ grains in any of the performed measurements. The IPF of the hexagonal phase was therefore not added.
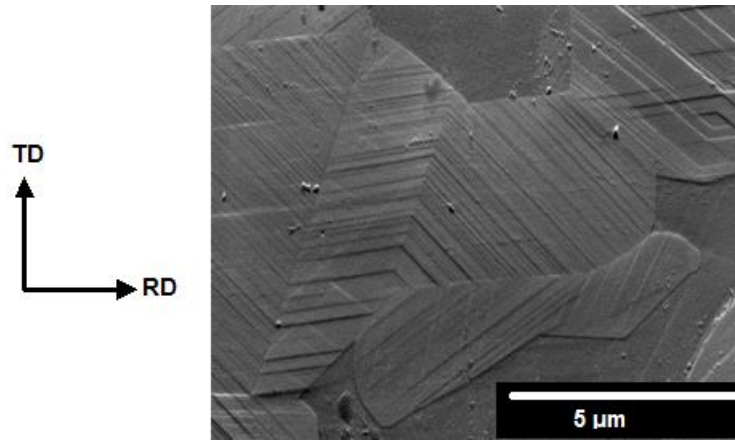
FIGURE 5. Microstructural surface changes after 18 h of electrochemical H charging of DSS: formation of slip bands in austenite.
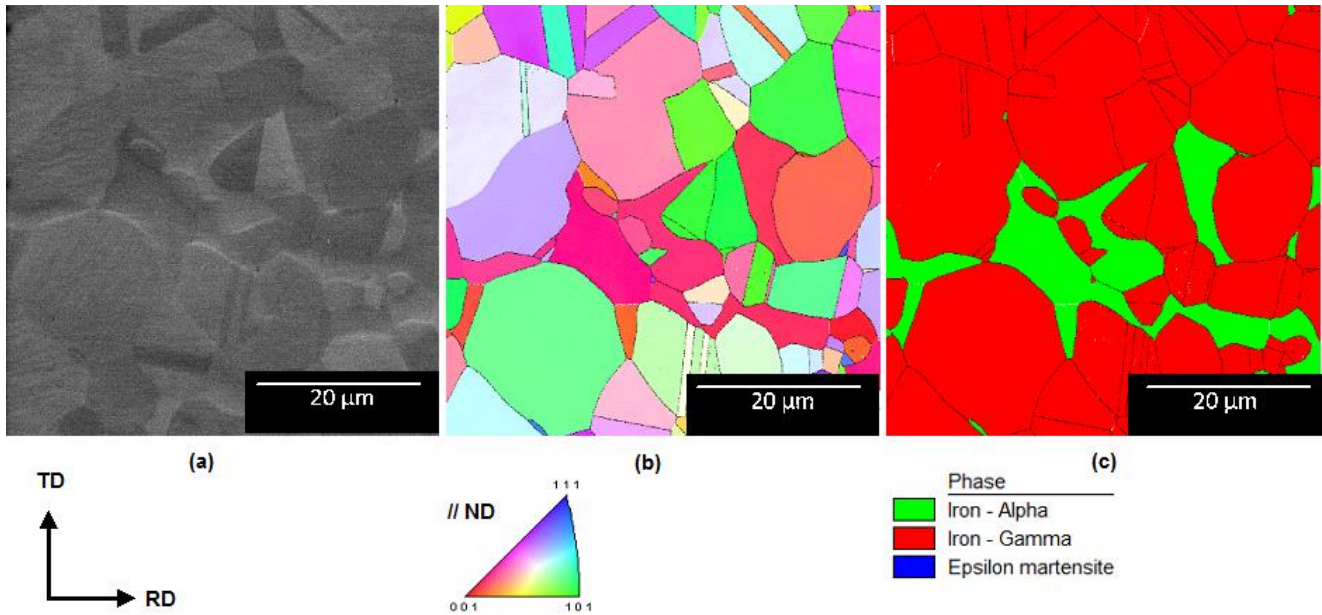

FIGURE 6. ND plane microstructure of DSS after 7 d of hydrogen charging and re-polishing: (a) SEM image, (b) ND IPF map, and (c) phase map.
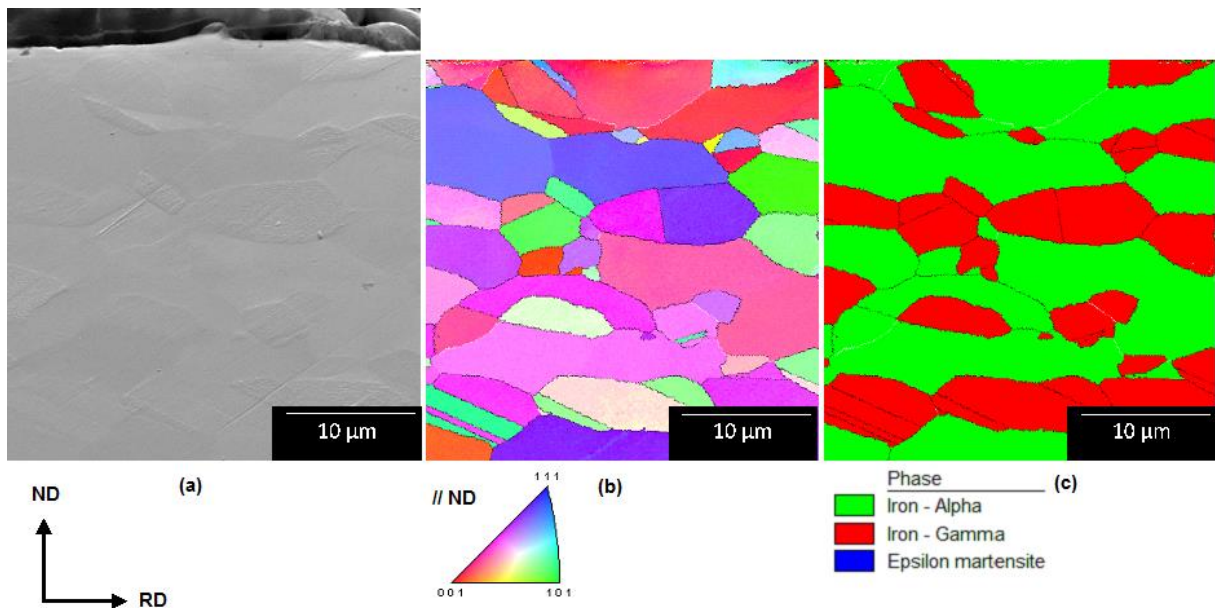

FIGURE 7. TD plane microstructure of DSS after 7 d of hydrogen charging: (a) SEM image, (b) ND IPF map, and (c) phase map

DISCUSSION

Electrochemical hydrogen charging has proven to be an efficient method for saturating BCC steels with hydrogen.[28] Hydrogen charging of duplex stainless steels is, however, more challenging due to the lower global hydrogen diffusion coefficient because of the presence of approximately 50 vol% of austenite, which has an inherent lower hydrogen diffusion coefficient compared to BCC phases. The experimental saturation curve was determined after reducing the thickness of the DSS plate to 0.3 mm which made it possible to determine a total hydrogen saturation level in a reasonable amount of time. Several days of electrochemical hydrogen charging in a sulphuric acid solution containing thiourea was still required to reach saturation. After approximately ten days of hydrogen charging, no significant increase in the total hydrogen content was observed, i.e., hydrogen saturation was reached for the given environment. The fitted model based on Fick's second law for diffusion resulted in a diffusion coefficient of 2.1×10^{-14} m²/s. This diffusion coefficient should be interpreted as an effective diffusion coefficient for the overall duplex stainless steel. Reported values in literature for the hydrogen diffusion coefficient of 2205 duplex stainless steel range from 2.2×10^{-14} m²/s to 6.4×10^{-14} m²/s.[29-32] The variations can be linked to differences in grain size, austenite phase fraction, and the relation between the hydrogen diffusion direction and the elongated grain direction in the DSS microstructure. Hydrogen diffusion will, for instance, be faster when it is parallel to the elongated grain structure.[32] Hydrogen diffusion in the present case was perpendicular to the elongated grains. A value at the lower end of the range could thus be expected. Apart from the effective diffusion coefficient, a hydrogen concentration at saturation of approximately 650 wppm was found from the model fit which is consistent with the measured experimental data. This hydrogen content is one to two orders of magnitude higher than typical values for BCC steels.[28,33] Reported literature data on hydrogen contents for DSS are in the same order of magnitude although no values as high as 650 wppm were mentioned. However, saturation, which was observed experimentally, was also never confirmed in literature. The theoretical equation for hydrogen diffusion (5) and the fitted effective diffusion coefficient, i.e., 2.1×10^{-14} m²/s, were therefore used to estimate saturation concentrations based on hydrogen concentrations found in literature for electrochemical hydrogen charging tests in similar electrolytes that were not continued until saturation. Dabah, et al.,[17] charged 156 wppm in a 0.6 mm plate after 72 h of charging. According to our theoretical model, 26.7% of the saturation concentration was reached with these parameters. The saturation concentration amounts to 583 wppm which is slightly lower than the value found in this work. The DSS was, however, heated to 450°C to determine the hydrogen concentration while in the present work, melt extraction was performed, thereby releasing more hydrogen. Zakroczymski, et al.,[24] detected 208 wppm in a 2.1 mm diameter DSS cylinder after 2 weeks of hydrogen charging. Considering the diffusion equation in cylindrical coordinates (6), the mean concentration in the cylinder similar to Eq. (5) for a plate material can be calculated (7).[34] With the used parameters, 30.8% of the saturation concentration was obtained according to the calculation. Saturation would then amount to 674 wppm which is very similar to the value found in the present work:

$$\frac{\partial C}{\partial t} = D \cdot \left(\frac{\partial^2 C}{\partial r^2} + \frac{1}{r}\frac{\partial C}{\partial r} \right) \ (6)$$

$$C = C_{HS} \cdot \left(1 - \frac{4}{R^2} \sum_{n=1}^{\infty} \frac{1}{\beta_n^2} \cdot \exp(-D \cdot \beta_n^2 \cdot t) \right)$$

$$\text{with } \beta_1 = \frac{2.405}{R}; \ \beta_2 = \frac{5.520}{R}; \ \beta_3 = \frac{8.654}{R}; \ \beta_4 = \frac{11.7915}{R}; \ R = \text{radius [m]} \ (7)$$

When the model based on Fick's second law for diffusion is applied to duplex stainless steels, the heterogeneous microstructure with a large discrepancy in hydrogen properties between the two phases has to be taken into account. The model gave a good estimation of the saturation time by defining an effective diffusion coefficient but was incapable of modeling the course of the curve before saturation. The assumption of constant concentration boundary conditions might not be entirely correct, especially in the beginning of the charging experiment. The experimental data showed a two-step increase in the hydrogen content with a steeper slope in the second part whereas the model showed a continuous increase as a function of charging time, cf. Figure 4. In duplex stainless steels, it can be assumed that hydrogen diffusion occurs mainly through the ferrite phase. Ferrite is a so-called highway for hydrogen transport. Turnbull and Hutchings[35] stated that the overall contribution of austenite to the diffusion flux in a duplex stainless steel is negligible in hydrogen permeation tests, despite the higher hydrogen solubility. Mente and Boellinghaus[36] constructed a FEM model for hydrogen diffusion in DSS taking into account the two-phase microstructure and found that ferrite was charged quickly followed by slow charging of the austenite phase. Ferritic stainless steels with compositions close to the composition of the present ferrite phase fraction are typically saturated in a time frame of hours, e.g., approximately 3 h were needed to saturate a 1 mm thick ferritic stainless steel plate which resulted in a fitted diffusion coefficient of 4.3×10^{-11} m²/s.[37] Owczarek and Zakroczymski[38] calculated values for the diffusion coefficient of ferrite and austenite separately in a DSS and found 1.5×10^{-11} m²/s for ferrite and 1.4×10^{-16} m²/s for austenite. A fully ferritic plate of 0.3 mm would then take approximately 1 h to saturate while a fully austenitic plate would need about 10 y to saturate (99% filled). However, as hydrogen is transported to all austenitic grains in the specimen thickness through the percolated ferrite phase, the austenite grains can be considered as thin plates with a thickness of 5 μm to which Eq. (5) can be applied. An austenite grain then needs 1.5 d to be saturated with hydrogen (99% filled) assuming hydrogen is charged from both sides. As the ferrite fraction should be saturated in 1 h with the calculated diffusion coefficient, the total charging time of the present duplex stainless steel should be approximately 1.5 d, i.e., the time needed for the austenite grains to be charged. However, at least 7 d were needed (Figure 3). Several factors might decelerate the diffusion process of hydrogen in ferrite of duplex stainless steels. Turnbull and Hutchings [35] stated that hydrogen diffusion in duplex stainless steels at moderate temperatures is dominated by trapping at the austenite/ferrite interface. These trapping events decelerate the permeation rate through the ferrite phase. Moreover, hydrogen has to surround the austenite islands. This results in longer effective diffusion paths. Owczarek and Zakroczymski[38] used a tortuosity factor to describe the deceleration of hydrogen diffusion by the austenite phase and found values of approximately 2 to 6 for a DSS with a membrane thickness of 0.3 mm, a grain size of 12 μm, 40 vol% of austenite, and hydrogen diffusion parallel to the elongated grains. In the present case, a more significant deceleration is expected as the DSS contains a higher austenite phase fraction. Moreover, hydrogen diffusion occurs perpendicular to the elongated grain.

The two-step increase in the experimental saturation curve is ascribed to the saturation of the ferrite phase fraction. During the first increase, ferrite is charged through the sample thickness. Given the high hydrogen concentration after several hours of charging, austenite grains close to the surface should be charged with hydrogen as well as ferrite has a too low a hydrogen solubility to explain the high values.[28] As stated, diffusion through ferrite is retarded in various ways. Several tortuosity factors and their resulting saturation time (99%) are given in Table 2. The

saturation times were obtained by inserting the sample thickness multiplied by the tortuosity factor as thickness 2l in Eq. (5) which can physically be interpreted by hydrogen that has to diffuse over a larger distance than the sample thickness because of the presence of austenite. If one assumes that ferrite is saturated after approximately 5 d (start of the change of slope), a factor of approximately 12 is needed which is reasonable given that a tortuosity factor of 6 is obtained for a less severe condition.[38] Moreover, as the austenitic phase is also charged and the austenite/ferrite interface can act as a trap, hydrogen charging of ferrite is additionally retarded apart from the tortuosity aspect. Once ferrite is saturated, hydrogen content of the austenite grains increases as hydrogen is no longer transported away through the ferrite phase and the austenite grains in the center are immediately charged from all sides. Therefore, the slope in the second step is expected to increase noticeably. Saturation is reached approximately 2 d after ferrite is saturated which is consistent with the saturation time for an austenite grain, based on the relevant diffusion coefficients.

TABLE 2. Ferrite Saturation Time for Different Retardation Factors

Retardation Factor		2	4	6	8	10	12	14
Saturation Time (h)		3	12	27	48	75	108	146

Many authors mentioned phase transformations during or after hydrogen charging of duplex stainless steels. In the present study, however, no martensitic phase transformations were observed. Most likely, the charging procedure was not severe enough to initiate phase transformations as other authors used higher current densities during electrochemical hydrogen charging. Nevertheless, the surface study revealed that other microstructural changes took place in the austenite phase during the first hours of hydrogen charging. Surface relief, consisting of various parallel lines with a certain spacing, was observed. The lines did not penetrate grain or phase boundaries. In some grains, parallel lines were formed in more than one direction (cf. Figure 5). Similar features were observed during plastic deformation of duplex stainless steel,[39-40] indicating that the phenomenon taking place can be linked to plastic deformation of the austenitic phase. Most likely, the surface relief can be attributed to the presence of slip bands arising from dislocation movement toward the surface. The surface relief was easily removed by a short polishing procedure. Typical slip band heights are about 20 to 30 Burger vectors,[41] which is consistent with the easy removal by polishing. Barnoush, et al.,[19] observed comparable surface changes with optical microscopy and atomic force microscopy during in situ electrochemical charging of super duplex stainless steel. These authors stated that a high enough hydrogen concentration reduces the shear modulus. Teus, et al.,[42] also reported that hydrogen reduced the shear modulus based on their density functional theory (DFT) calculations. Due to the lowered shear modulus, Frank-Read sources start producing new dislocations under the high internal stress inherent to duplex stainless steels. Duplex stainless steels are indeed quenched from very high temperatures at which the phase balance is ideal. The large difference in thermal expansion coefficient between the two phases results in high tensile stresses in the austenite phase and high compressive stresses in the ferrite phase.[43] Consequently, newly emerged and already existing dislocations start migrating and the ones reaching the surface produce the surface relief known as slip bands. Luo, et al.,[20] observed similar features in the austenite phase by combining EBSD and ECCI analyses of DSS samples exposed to hydrogen charging and concluded that the lines were caused by dislocations that developed into stacking faults rather than into slip bands. Other proof for dislocation nucleation during hydrogen charging of duplex stainless steels has been given by Liang, et al.,[21] who measured the dislocation density of a super duplex stainless steel with ToF neutron diffraction. They observed an increase in dislocation density with one order of magnitude in austenite after hydrogen charging. It should also be noted that dislocation movement can be facilitated in the presence of hydrogen as proposed by the hydrogen enhanced localized plasticity (HELP) model.[33,44] Dislocation nucleation and migration is, however, not a continuous event over the charging procedure. The dislocation density typically reaches a saturation level because dislocation movement is hindered by obstacles and other dislocations. Moreover, the available stress level is limited as there is no externally applied stress and dislocation movement results in stress relief. In situ measurements indeed showed that the evolution of slip lines seemed to stop or slow down.[19] It should be noted that dislocation density might also have increased in the ferrite phase due to hydrogen charging as there are high internal stresses in the ferrite phase as well. Liang, et al.,[21] observed an increase in the dislocation density in the ferrite of a super DSS with neutron diffraction. The increase was, however, not as large as in the austenite phase. Luo, et al.,[45] observed enhanced dislocation movement and dislocation multiplication in the ferrite phase fraction of 2205 DSS due to absorbed hydrogen as well. Fréchard, et al.,[39] performed tensile tests on DSS and mentioned that austenite showed multiple slip bands while ferrite showed no slip bands in the beginning and a limited amount of slip bands close to the austenite phase boundary at higher strain levels. Two distinct reasons can therefore be considered for the absence of lines in the ferrite grains in our samples. First, the stress level was possibly insufficient for slip band formation in ferrite. Second, the observed lines in the austenite grains are stacking faults. Dislocations do not develop into stacking faults in ferrite due to the higher stacking fault energy.

The overall increase in the dislocation density in both the austenite and ferrite phase due to hydrogen charging resulted most likely in a higher hydrogen concentration compared to the initial state as dislocations act as trapping sites for hydrogen atoms and thus increase the hydrogen solubility of a material, however, in the austenitic phase, the increase in the hydrogen concentration due to trapping sides provided by cold work is not very large.[46] The increase in dislocation density cannot be avoided as the high internal stresses, providing the necessary stress level for dislocation nucleation, are inherent to the production process of duplex stainless steels. The applied experimental methodology in this work can, therefore, be considered as a reliable procedure to saturate duplex stainless steels with hydrogen as no damage in the form of cracks or martensite formation was observed which would affect hydrogen diffusion and hydrogen trapping to a much larger extent.

CONCLUSIONS

- ❖ A total hydrogen concentration of approximately 650 wppm was reached at saturation for UNS S32205 duplex stainless steel. An effective diffusion coefficient of 2.1×10^{-14} m²/s was determined, which was consistent with values found in literature.
- ❖ A two-step increase in hydrogen concentration was observed as a function of charging time. This was explained by consecutive saturation 2.1 of the ferrite phase fraction and the austenite islands.
- ❖ When high hydrogen concentrations were accompanied with high internal stresses, as inherent to duplex stainless steels, dislocation sources became active and the dislocation density increased both in the austenite and ferrite. This was determined by

microstructural analysis for specific hydrogen charging times. Slip bands were observed in the austenite phase fraction, which were correlated to dislocation generation and movement.

ACKNOWLEDGMENTS

REFERENCES

1. I. Alvares-Armas, S. Degallaix-Moreuil, *Duplex Stainless Steels*, (London: John Wiley & Sons, 2009).
2. A. El-Yagzi, D. Hardie, *Corros. Sci.* 38, 5 (1996): p. 735-744.
3. F. Zucchi, V. Grassi, C. Monticelli, G. Trabanelli, *Corros. Sci.* 48 (2006): p. 522-530.
4. J. Woodtli, R. Kieselbach, *Eng. Fail. Anal.* 7 (2000): p. 427-450.
5. T. Depover, K. Verbeken, *Mater. Sci. Eng. A* 669 (2016): p. 134-149.
6. T. Depover, E. Wallaert, K. Verbeken, *Mater. Sci. Eng. A* 649 (2016), p. 201-208.
7. S. Chan, *J. Chin. Inst. Eng.* 22, 1(1999): p. 43-53.
8. H. Bhadeshia, *ISIJ Int.* 56, 1 (2016): p. 24-36.
9. T. Depover, E. Wallaert, K. Verbeken, *Mater. Sci. Eng. A* 664 (2016): p. 195-205.
10. E. Herms, J. M. Olive, M. Puiggali, *Materials Sci. Eng. A* 272, 2 (1999): p. 279-283.
11. M. Hatano, M. Fujinami, K. Arai, H. Fujii, M. Nagumo, *Acta Mater*. 67 (2014): p. 342-353.
12. T. Michler, C. San Marchi, J. Naumann, S. Weber, M. Martin, *Int. J. Hydrog. Energy* 37 (2012): p. 16231-16246.
13. V. Olden, R. Johnsen, *Mater. Des.* 29 (2008): p. 1934-1948.
14. S. Matsuoka, J. Yamabe, H. Matsunaga, *Eng. Fract. Mech.* 153 (2016): p. 103-127.
15. Q. Yang, J. Luo, *Mater. Sci. Eng. A* 288 (2000): p. 75-83.
16. A. Glowacka, M. Wozniak, W. Swiatnicki, *J. Alloys Compd.* 404-406 (2005): p. 595-598.
17. E. Dabah, V. Lisitsyn, D. Eliezer, *Mater. Sc. Eng. A* 527 (2010): p. 4851-4857.
18. A. Glowacka, M. Wozniak, G. Nolze, W. Swiatnicki, *Solid State Phenom.* 112(2006): p. 133-140.
19. A. Barnoush, M. Zamanzade, H. Vehoff, *Scripta Mater.* 62 (2010): p. 242-245.
20. H. Luo, C. Dong, Z. Liu, M. Maha, X. Li, *Mater. Corros.* 64,1 (2013).
21. X. Liang, M. Dodge, S. Kabra, J. Kelleher, T. Lee, H. Dong, *Scripta Mater.* 143 (2018): p. 20-24.
22. C. San Marchi, B. Somerday, J. Zelinski, X. Tang, G. Schiroky, *Metall. Mater. Trans. A* 38A (2007): p. 2763-2775.
23. A. El-Yazgi and D. Hardie, *Mater. Sci. Technol.* 16 (2000): p. 506-510.
24. T. Zakroczymski, A. Glowacka, W. Swiatnicki, *Corros. Sci.* 47 (2005): p. 1403-1414.
25. A. Griffiths, A. Turnbull, *Corros. Sci.* 53 (1997): p. 700-704.
26. V. Randle, *Mater. Charact.* 60 (2009): p. 913-922.
27. J. Crank, *The Mathematics of Diffusion* (Oxford: Oxford University press, 1975).
28. T. Depover, O. Monbaliu, E. Wallaert, K. Verbeken, *Int. J. Hydrog. Energy* 40 (2015): p. 16977-16984.
29. W. Luu, P. Liu, P. Wu, *Corros. Sci.* 44 (2002): p. 1783-1791.
30. S. Chen, T. Wu, J. Wu, *J. Materials Sci.* 39 (2004): p. 67-71.
31. S.-L. Chou, W.-T. Tsai, *Mater. Sci. Eng. A* 270 (1999): p. 219-224.
32. J. Zelinski, C. San Marchi, "Technical Reference on Hydrogen Compatibility of Materials: High Alloy Ferritic Steels: Duplex Stainless Steels" (Livermore: Sandia National Laboratories, 2008).
33. T. Depover, K. Verbeken, *Corros. Sci.* 112 (2016): p. 308-326.
34. R. Barrer, *Diffusion In and Through Solids* (Cambridge: The University Press, and Macmillan, 1941).
35. A. Turnbull, R. Hutchings, *Mater. Sci. Eng. A* 177 (1994): p. 161-171.
36. T. Mente, T. Boellinghaus, *Weld. World* 56 (2012): p. 66-78.
37. E. Malitckii, Y. Yagodzinskyy, P. Lehto, H. Remes, J. Romu, H. Hänninen, *Mater. Sci. Eng. A* 700 (2017): p. 331-337.
38. E. Owczarek, T. Zakroczymski, *Acta Mater.* 48 (2000): p. 3059-3070.
39. S. Fréchard, F. Martin, C. Clément, J. Cousty, *Mater. Sci. Eng. A* 418 (2006): p. 312-319.
40. I. Serre, D. Salazar, J.-B. Vogt, *Mater. Sci. Eng. A* 492 (2008): p. 428-433.
41. U. Kocks, H. Mecking, *Prog. Mater. Sci.* 48 (2003): p. 171-273.
42. S. Teus, V. Shivanyuk, B. Shanina, V. Gavriljuk, *Phys. Status Solidi* 204, 12 (2007): p. 4249-4258.
43. S. Harjo, Y. Tomota, M. Ono, *Acta Mater.* 47, 1 (1999): p. 353-362.
44. K. Nibur, D. Bahr, B. Somerday, *Acta Mater.* 54 (2006): p. 2677-2684.
45. H. Luo, Z. Li, Y.-H. Chen, D. Ponge, M. Rohwerder, D. Raabe, *Electrochem. Commun.* 79 (2017): p. 28-32.
46. G. Thomas, "Hydrogen Trapping in FCC Metals," in International Conference on Effects of Hydrogen on Materials (Warrendale, Pa. : Metallurgical Society of AIME, 1981).